Structural Transformation and Low-Pressure Catalysis for Ethyl Acetate Hydrogenation of Rh/One-Atomic-Layer GeO_2/SiO_2

Kazu Okumura,[†] Kiyotaka Asakura,[‡] and Yasuhiro Iwasawa*[,†]

Department of Chemistry, Graduate School of Science, The University of Tokyo, Hongo, Bunkyo-ku, Tokyo 113, Japan, and Research Center for Spectrochemistry, Faculty of Science, The University of Tokyo, Hongo, Bunkyo-ku, Tokyo 113, Japan

Received: May 5, 1997; In Final Form: August 3, 1997[⊗]

We prepared a new Rh/one-atomic-layer GeO_2/SiO_2 catalyst by supporting $Rh_6(CO)_{16}$ precursor on the one-atomic-layer GeO_2/SiO_2. The obtained catalyst was active for conversion of ethyl acetate to ethanol by H_2 reduction under mild reaction conditions. Three different structures and chemical states of Rh species on the one-atomic-layer GeO_2/SiO_2, characterized by EXAFS, TPD, TEM, and FT-IR, were formed depending on the prereduction temperature, Rh carbonyl cluster, Rh metal, and RhGe alloy. The Rh atoms in the metallic state were most active for the ethanol formation. The one-atomic-layer GeO_2 was much more effective as support for the Rh metallic particles than three-dimensional GeO_2 particles dispersed on SiO_2. Rh/bulk-GeO_2 and Rh/SiO_2 were inactive for this reaction. Ethyl acetate dissociatively adsorbed on the one-atomic-layer GeO_2, while hydrogen adsorbed on the Rh metallic particles. The present study exemplifies the advantageous applications of an inorganic oxide monolayer to preparation of supported metal catalysts.

1. Introduction

One-atomic-layer oxides have been demonstrated to provide a new kind of support for metals and also new catalysis.[1−6] Spread of monolayer oxides on, for example, SiO_2 not only increases the surface area of the oxides but also makes it easy to characterize the topmost surface of oxides relevant to the catalytic phenomena. Metal−support interaction may be well characterized compared to that in metal−bulk oxide systems. Recently, we prepared Rh particles/one-atomic-layer GeO_2/SiO_2 (the amount of GeO_2 is less than a monolayer) by the reaction of $Ge(OMe)_4$ with surface OH groups of SiO_2 followed by calcination at 673 K and by the reaction of a Rh dimer complex with isolated OH groups of the obtained one-atomic-layer GeO_2 on SiO_2 followed by reduction with H_2 at 423−723 K. Behaviors of Rh and Ge atoms in the Rh/one-atomic-layer GeO_2/SiO_2 were entirely different from those in Rh/bulk-GeO_2 during the reduction, as characterized by EXAFS, XRD, and FT-IR.[7] The aim of this study is (1) to prepare a new Rh/one-atomic-layer GeO_2/SiO_2 catalyst by using the $Rh_6(CO)_{16}$ cluster as a precursor, (2) to examine structural transformations of the Rh/one-atomic-layer GeO_2/SiO_2 sample during reduction with H_2 at various temperatures, and (3) to apply the new Rh/one-atomic-layer GeO_2/SiO_2 to a selective catalytic hydrogenation.

In this study the hydrogenation of ethyl acetate to ethanol was chosen as a target catalytic reaction. Ge has the potential to promote hydrogenation reactions that occur on noble metals. For instance, the addition of 3 atom % Ge to Pt particles increases the activity and selectivity in the selective hydrogenation of α,β-unsaturated aldehyde to unsaturated alcohol.[8] Catalytic hydrogenation of esters to the corresponding alcohols has been practiced for many years. Copper chromite is a current commercial hydrogenation catalyst and has been applied to the production of diols from diesters or the production of methanol from carbon monoxide and hydrogen by two-stage processes.[9,10] In the two-step methanol synthesis the first step involves CO insertion into the O−H bond of methanol to form methyl formate, and in the following second step a methyl formate molecule is hydrogenated to two methanol molecules. This process is thermodynamically superior to the conventional direct hydrogenation of CO.[11−13] In commercial processes, copper chromite is used at pressures as high as 23 MPa and 423−573 K, but this catalyst is not so stable and is deactivated. Thermodynamic calculations show that this reaction can proceed under more mild conditions such as atmospheric pressure and moderate temperatures lower than 500 K. Recently, several groups have developed new catalysts for ester hydrogenation. Grey et al. have conducted hydrogenation reactions in solution by using a soluble anionic ruthenium hydride complex as catalyst.[14] Basset and his co-workers have reported the catalytic property of RhSn alloy catalysts for the ethyl acetate hydrogenation at low-pressure conditions.[15,16] Wehner et al. used Pd/ZnO which is also known to be active for methanol synthesis in CO hydrogenation.[17] Desh et al. reported a Ru−Sn boride catalyst to be active for the hydrogenation of long chain fatty acids.[18] In addition to the hydrogenation of esters, hydrogenation of acid anhydrides has also been studied; a typical example is the highly regioselective reduction of asymmetrical cyclic carboxylic acid anhydrides to g-lactones.[19]

We have found the excellent catalytic property of the Rh/one-atomic-layer GeO_2/SiO_2 sample in the ethyl acetate hydrogenation to ethanol under mild reaction conditions. The activity and selectivity of this catalyst were entirely different from those of Rh/bulk-GeO_2, Rh/SiO_2, and Rh/three-dimensional GeO_2 particles/SiO_2. The new Rh/one-atomic-layer GeO_2/SiO_2 catalyst was characterized by EXAFS, TPD, and FT-IR. The present study demonstrates the advantageous application of an inorganic−oxide monolayer as a new class of catalyst.

2. Experimental Section

2.1. Catalyst Preparation. Preparation of one-atomic-layer GeO_2 supported on SiO_2 will be reported elsewhere,[20] but is summarized briefly. $Ge(OMe)_4$ as precursor was purchased from Soekawa Chemicals Co. (99.999%) and purified by

* Corresponding author. Fax: 81-3-5800-6892 or 81-3-3814-2627. E-mail: iwasawa@utsc.s.u-tokyo.ac.jp.
† Department of Chemistry.
‡ Research Center for Spectrochemistry.
⊗ Abstract published in *Advance ACS Abstracts,* November 15, 1997.

S1089-5647(97)01515-0 CCC: $14.00

distillation in a vacuum line before use. SiO_2 (Aerosil 300; 300 m^2 g^{-1}) was evacuated at 473 K for 1 h to remove physisorbed water and exposed to given amounts of $Ge(OMe)_4$ vapor at 393 K for 1 h, followed by evacuation at 473 K to remove the unreacted $Ge(OMe)_4$ and the organic products. The obtained sample was calcined at 693 K for 1 h under 20.0 kPa of oxygen in a closed circulating system. The evolved CO_2 and H_2O were removed by a trap with liquid N_2. Loading of Ge in the GeO_2/SiO_2 was fixed at 7.4 wt %.

Hexarhodium hexadecacarbonyl $Rh_6(CO)_{16}$ (purity: 98%) was purchased from Aldrich Chemical Co. and used without further purification. Chloroform was purified by reflux over 5 Å molecular sieves and distillation before use as solvent for $Rh_6(CO)_{16}$. A chloroform solution of $Rh_6(CO)_{16}$ was stirred vigorously with the one-atomic-layer GeO_2/SiO_2 under Ar atmosphere at room temperature. No decolorization of the solution was observed during stirring, which suggests that reaction of $Rh_6(CO)_{16}$ with the one-atomic-layer GeO_2/SiO_2 seemed not to take place significantly at room temperature. Therefore the solvent was removed by evaporation to enforce the support of $Rh_6(CO)_{16}$ on the one-atomic-layer GeO_2/SiO_2. $Rh_6(CO)_{16}$ was also supported on SiO_2 (Aerosil 300) and GeO_2 (hexagonal type; Wako Pure Chemical Co.) in a similar manner to the case of the GeO_2/SiO_2. The loading of Rh in every catalyst was fixed at 2.0 wt %. The samples were reduced at given temperatures for 2 h under 13.3 kPa of hydrogen without calcination of the incipient supported $Rh_6(CO)_{16}$ samples.

2.2. Rh K-Edge and Ge K-Edge XAFS Measurement. X-ray absorption fine structure (XAFS) spectra at Rh and Ge K-edges were measured at room temperature in a transmission mode at the beam lines 10B and 7C of Photon Factory in the National Laboratory for High-Energy Physics (KEK-PF), respectively (Proposal No. 94G-203). The storage ring energy was operated at 2.5 GeV with a ring current of 250−350 mA. The 10B and 7C stations are equipped with a Si(311) channel cut monochromator and a Si(111) sagittal focusing double-crystal monochromator, respectively. To remove the higher harmonics, the Si(111) monochromator was detuned to 70%. The sample was transferred to glass cells with two Kapton windows connected to a closed circulating system without contacting air. For the measurement of Rh K-edge spectra two ion chambers filled with Ar and Kr were used as detectors for I_0 and I, respectively, while two ion chambers filled with 100% N_2 and 15% Ar/85% N_2 were used for the measurement of Ge K-edge spectra.

For EXAFS analysis, the oscillation was first extracted from the EXAFS data by a spline smoothing method.[21] The oscillation was normalized by the edge height around 50 eV above the threshold. The energy dependence of edge height was corrected by the McMaster equation.[22] The Fourier transformation of the k^3-weighted EXAFS oscillation from k space to r space was performed over the range 30−140 nm^{-1} to obtain a radial distribution function. The inversely Fourier filtered data were analyzed by a curve fitting method based on eq 1.

$$\chi(k) = \sum N_j F_j(k) \exp(-2\sigma_j^2 k_j^2) \sin(2kr_j + \phi_j(k))/kr_j^2 \quad (1)$$

where N_j, r_j, and σ_j represent coordination number, bond distance, and Debye−Waller factor, respectively. $F_j(k)$ and $\phi_j(k)$ are amplitude and phase shift functions, respectively. For the curve fitting analysis, the empirical phase shift and amplitude functions for Rh−Rh, Ge−Ge, Rh−O and Ge−O were extracted from the data for Rh metal, Ge metal, Rh_2O_3, and GeO_2 (hexagonal), respectively. The theoretical parameters used for the fitting of Rh−Ge and Ge−Rh bonds as well as Rh−C_t (terminal CO in $Rh_6(CO)_{16}$) and Rh−C_b (μ^3-CO in $Rh_6(CO)_{16}$) were calculated by FEFF6.0. Error bars in the analysis were estimated by the R factor (R_f) determined by eq 2.

$$R_f = \sqrt{\sum (k^3\chi_{cal} - k^3\chi_{obs})^2/(k^3\chi_{obs})^2} \quad (2)$$

The degree of error bars in the present curve fitting analysis for bond distance and coordination number is estimated to be 0.003 nm and 20%, respectively. The analysis of EXAFS data was performed by using the "REX" program (RIGAKU).

2.3. Temperature Programmed Desorption. Temperature-programmed desorption was carried out under hydrogen (13.3 kPa) in a closed circulating system. The temperature was raised from room temperature to 773 K at a heating rate of 4 K min^{-1}. The desorbed products were analyzed with a gas chromatograph (Shimadzu GC-8A; Column 5 Å molecular sieve).

2.4. Catalytic Hydrogenation of Ethyl Acetate. Catalytic hydrogenation reactions of ethyl acetate over 0.1 g of catalyst were conducted in a closed circulating system equipped by a gas chromatograph. Reduction of the catalyst was conducted under hydrogen at 13.3 kPa and at given temperatures (473−723 K) for 2 h in situ before use as catalysts, followed by evacuation at the same temperatures. The ethyl acetate was purified by repeated freeze−thaw cycles. The catalytic reactions were conducted under a mixture of 6.6 kPa of hydrogen and 1.3 kPa of ethyl acetate. The reaction temperature was fixed at 473 K. The products were analyzed by a gas chromatograph using a DOS column for analysis of ethanol and acetaldehyde and a VZ-10 column for analysis of methane and ethane.

2.5. Measurement of FT-IR Spectra. FT-IR spectra were measured on a JASCO FT-IR 230 spectrometer with 2 cm^{-1} resolution. The samples were pressed to thin wafers of 20 mm and placed in a holder in an in situ IR cell combined in a closed circulating system. The samples, Rh/one-atomic-layer GeO_2/SiO_2, GeO_2/SiO_2, GeO_2, and SiO_2, were exposed to 6.6 kPa of ethyl acetate at various temperatures in the range 373−473 K, followed by evacuation.

3. Results and Discussion

3.1. Structure of One-Atomic-Layer GeO_2/SiO_2. Here we briefly summarize the structure of one-atomic-layer GeO_2/SiO_2 determined by FT-IR, XRD, and EXAFS.[20] When $Ge(OMe)_4$ reacted with the pretreated SiO_2 (surface area = 300 m^2/g), a maximum loading of Ge was 7.4 wt %, which corresponded to 0.2 monolayer (or 2 Ge nm^{-2}). FT-IR studies revealed that the isolated silanols (3745 cm^{-1}) disappeared after the deposition of $Ge(OMe)_4$, indicating the reaction between $Ge(OMe)_4$ and the isolated silanol group took place preferentially. After the calcination at 693 K, two peaks appeared at 3745 and 3676 cm^{-1} with almost the same height. The former can be attributed to the silanols and the latter one to the isolated OH groups on the GeO_2 overlayer. The 7.4 wt % GeO_2/SiO_2 showed no XRD peak except a broad one due to the SiO_2, while strong GeO_2 XRD peaks appeared after the exposure of the same sample to moisture at room temperature. Curve fitting analysis for the Ge K-edge EXAFS data of the one-atomic-layer GeO_2/SiO_2 in Figure 6 revealed the presence of Ge−O and Ge−Ge at 0.173 and 0.311 nm, respectively. The interatomic bond distances are in agreement with those for a hexagonal type GeO_2 rather than tetragonal GeO_2, indicating the local structure of the GeO_2 layer is similar to the hexagonal GeO_2 structure. The small Ge−Ge coordination number of 2.0 compared with 4 for the hexagonal GeO_2 is compatible with a layer structure originating from the chemical vapor deposition reaction of $Ge(OMe)_4$ with the surface OH groups of SiO_2.

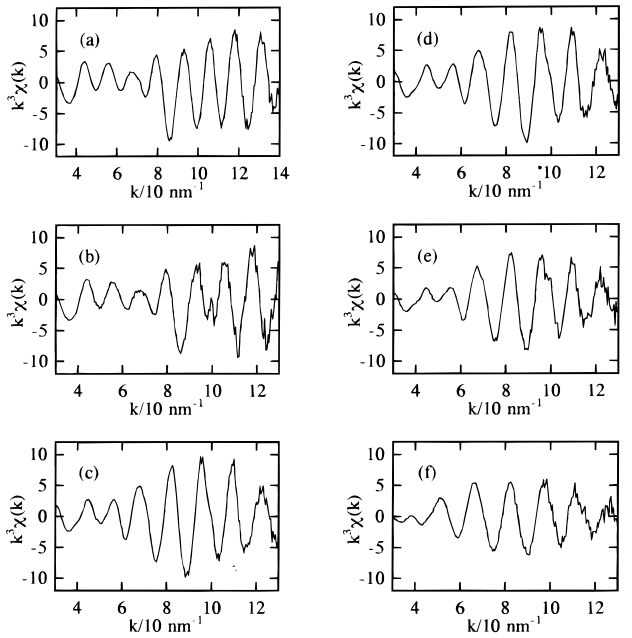

Figure 1. Rh K-edge EXAFS $k^3\chi(k)$ oscillations for $Rh_6(CO)_{16}$ (a) and Rh/one-atomic-layer GeO_2/SiO_2 (b-f); (b) incipient supported $Rh_6(CO)_{16}$, (c) reduced at 423 K, (d) reduced at 523 K, (e) reduced at 623 K, and (f) reduced at 723 K.

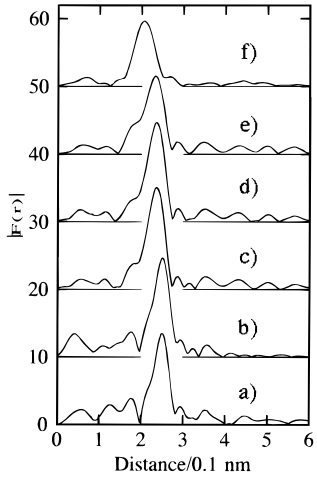

Figure 2. Rh K-edge EXAFS Fourier transforms for $Rh_6(CO)_{16}$ (a) and Rh/one-atomic-layer GeO_2/SiO_2 (b-f). a-f correspond to Figure 1.

3.2. Structural Change of $Rh_6(CO)_{16}$ during Reduction Treatments Determined by XAFS Spectroscopy. Figure 1 shows Rh K-edge EXAFS spectra for the $Rh_6(CO)_{16}$ cluster, the incipient supported $Rh_6(CO)_{16}$ on one-atomic-layer GeO_2/SiO_2, and the Rh/one-atomic-layer GeO_2/SiO_2 sample reduced with H_2 at 423−723 K. The incipient supported $Rh_6(CO)_{16}$ shows EXAFS data similar to those for the $Rh_6(CO)_{16}$ cluster itself (Figures 1 and 2), and the curve fitting analysis in Figure 3 and Table 1 reveals that the framework of the Rh carbonyl cluster is retained on the GeO_2/SiO_2 surface. The isolated Ge−OH peak in the FT-IR spectrum decreased and shifted to the lower wavenumber side due to hydrogen bonding with the cluster, while Si−OH peaks did not change significantly upon supporting $Rh_6(CO)_{16}$. It seems that $Rh_6(CO)_{16}$ preferentially interacts with the one-atomic-layer GeO_2 (1/5 ML) rather than the exposed SiO_2 surface.

The EXAFS feature changed by reduction with H2 at 423 K (Figure 1c). The single peak around 0.25 nm (phase shift uncorrected) observed in the Fourier transform shifted toward the shorter length, as shown Figure 2c. The Rh−Rh bond length

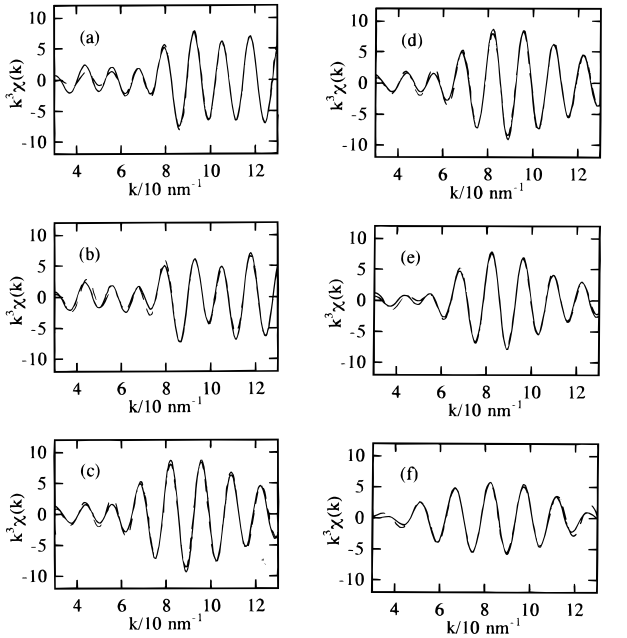

Figure 3. Curve fitting analysis for Rh K-edge EXAFS spectra for $Rh_6(CO)_{16}$ (a) and Rh/one-atomic-layer GeO_2/SiO_2 (b-f) (a-f are the same as in Figure 1): (a, b) analysis with Rh−Ct, Rh−Cb, and Rh−Rh three waves; (c,d) analysis with Rh−Rh single wave; (e) analysis with Rh−Rh and Rh−Ge two waves; (f) analysis with Rh−Ge single wave.

TABLE 1: Curve Fitting Results of Rh K-Edge EXAFS Spectra for $Rh/GeO_2/SiO_2$

sample	scatterer atom	CN[a]	r/nm[b]	ΔE_0/eV[c]	σ/nm[d]	R_f/%[e]
incipient supported $Rh_6(CO)_{16}$	C	2.1	0.186	0.8	0.0054	5.6
	C	2.0	0.217	0.8	0.0054	
	Rh	2.8	0.280	0.9	0.0059	
reduced at 423 K	Rh	7.4	0.266	−9.0	0.0085	1.8
reduced at 523 K	Rh	7.5	0.266	−9.1	0.0085	1.8
reduced at 623 K	Rh	3.7	0.268	−6.6	0.0074	0.9
	Ge	0.9	0.241	−5.9	0.0049	
reduced at 723 K	Ge	3.5	0.244	−5.8	0.0086	2.5

[a] Coordination number. [b] Bond distance. [c] Difference in the origin of photoelectron energy between the reference and the sample. [d] Debye−Waller factor. [e] Residual factor.

TABLE 2: One-Wave Curve Fitting Results of Ge K-Edge EXAFS Spectra for Rh/One-Atomic-Layer GeO_2/SiO_2

reduction temperature/K	scatterer atom	CN[a]	r/nm[b]	ΔE_0/eV[c]	σ/nm[d]	R_f/%[e]
723	Rh	0.7	0.243	−3.9	0.0099	10.7

[a] Coordination number. [b] Bond distance. [c] Difference in the origin of photoelectron energy between the reference and the sample. [d] Debye−Waller factor. [e] Residual factor.

was determined to be 0.266 nm by the curve fitting (Table 1), which is close to the Rh−Rh bond distance of Rh metal (0.269 nm). Besides the decrease in the Rh−Rh bond distance from 0.280 nm to 0.266 nm, the $Rh-C_t$ and $Rh-C_b$ bonding disappeared with Rh/one-atomic-layer GeO_2/SiO_2 reduced at 423 K, as shown in Table 1.

Desorption of CO from the incipient supported $Rh_6(CO)_{16}$ was examined by TPD under hydrogen as shown in Figure 4. A small desorption peak at 390 K may correspond to the change in the EXAFS spectra. However, two major desorption peaks were observed at 550−650 K in Figure 4, and the amount of CO desorbed around 390 K was only 8% of the total amount of desorbed CO in TPD. The desorption feature may be

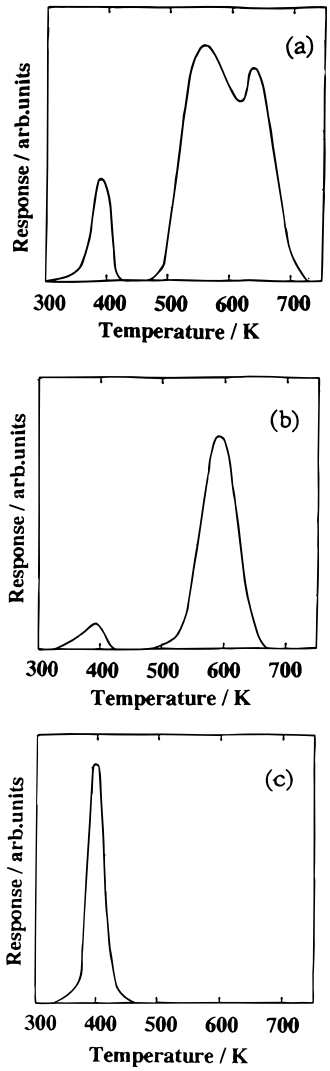

Figure 4. Temperature-programmed desorption of CO under 13.3 kPa of H_2: (a) Rh/one-atomic-layer GeO_2/SiO_2, (b) Rh/SiO_2, (c) Rh/bulk-GeO_2; heating rate 4 K min^{-1}.

incompatible with the EXAFS results in Table 1. The EXAFS data for the samples reduced at higher temperatures than 423 K demonstrate destruction of the cluster framework accompanied with decarbonylation of the supported $Rh_6(CO)_{16}$ and aggregation of the Rh_6 cluster to small Rh particles with the coordination number of 7.4−7.5 for the Rh−Rh bond. The average sizes of Rh particles in the Rh/one-atomic-layer GeO_2/SiO_2 catalysts reduced at 523 and 723 K were estimated to be 2.6 and 2.8 nm, respectively, by transmission electron microscopy (TEM). The decarbonylation process is not a simple desorption process because the majority of the carbonyl ligands did not desorb below 500 K. We propose that the Rh_6 cluster on the GeO_2/SiO_2 is transformed to small Rh particles by partial decarbonylation before full decarbonylation. The mechanism of the partial decarbonylation-induced structural transformation is not clear at present, and the structure and shape of the produced Rh clusters/particles cannot be characterized by EXAFS and FT-IR. The peak for adsorbed CO was not observed under the catalytic reaction conditions (see Figure 8c).

The peak intensity in the Fourier transform decreased by reduction of the sample at 623 K, as shown in Figure 2e. This is not due to redispersion of Rh particles because the Rh particle size did not change significantly in the temperature range 523−723 K. The reduction of the peak height in the Fourier transform can be explained by RhGe particle formation. In fact,

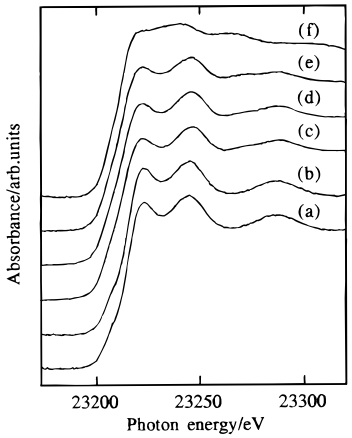

Figure 5. Rh K-edge XANES spectra of (a) $Rh_6(CO)_{16}$ and (b-f) Rh/one-atomic-layer GeO_2/SiO_2: (b) incipient supported species, (c) reduced at 423 K, (d) reduced at 523 K, (e) reduced at 623 K, (f) reduced at 723 K.

the curve fitting analysis of the $k^3\chi(k)$ spectrum of this sample using a Rh−Rh single wave never reproduced the observed data, and good fitting was obtained by the addition of a Rh−Ge wave, as shown in Figure 3e. The Rh−Rh and Rh−Ge distances were determined to be 0.268 and 0.241 nm, respectively, as shown in Table 1. The peak in the Fourier transform for Rh/GeO_2/SiO_2 reduced at 723 K (Figure 2f) shifted toward a shorter distance. As for this sample, the curve fitting based on the Rh−Ge one wave gave the best result (Figure 3f and Table 1). The fitting was not improved by two-wave (Rh−Ge and Rh−Rh) analysis. These results suggest the formation of RhGe alloy particles on the GeO_2/SiO_2. The determined Rh−Ge bond distance was 0.244 nm, which is essentially the same as 0.241 nm for Rh−Ge in the sample reduced at 623 K, while the coordination number of the Rh−Ge bond increased from 0.9 to 3.5 as the reduction temperature increased from 623 to 723 K, respectively. The change in the bonding modes of Rh−Rh and Rh−Ge indicates a gradual RhGe alloy formation of the metallic Rh particles with the reduced one-atomic-layer GeO_2 on SiO_2. These results are different from those on RhGe alloys prepared by the deposition of Rh dimer complex $[Rh(C_5Me_5)Me]_2(\mu\text{-}CH_2)_2$ and successive calcination and reduction treatment, where Rh−Rh bonding was always observed. The reason may be referred to the difference of Rh particle size. The $Rh_6(CO)_{16}$-derived catalyst was prepared by reduction with H_2 without oxidation before the reduction, while the Rh dimer-derived sample was prepared by reduction after oxidation of the incipient supported species.

Figure 5 shows the XANES spectra of $Rh_6(CO)_{16}$, the incipient supported $Rh_6(CO)_{16}$, and the reduced Rh/one-atomic-layer GeO_2/SiO_2. The peaks at 10 and 35 eV above the threshold energy attenuated with a rise of reduction temperature, which is evident in the spectrum of the sample reduced at 723 K. The first peak is related to the electronic transitions from the core level (1s) to the empty states above the Fermi level, and the second peak is due to the multiple scattering processes of the outgoing electron.[23] The calculation of multiple scattering in different cluster sizes shows the increase of the second peak with an increase in particle size.[24] The observed attenuation of the peak intensity may be due to the formation of RhGe alloy particles, where Rh atoms are replaced by Ge atoms and the back scattering of photoelectrons by Ge atoms is less than that by Rh atoms.

Figure 6a shows the Ge K-edge EXAFS spectra of Rh/one-atomic-layer GeO_2/SiO_2 reduced at 723 K and one-atomic-layer GeO_2/SiO_2. To extract the contribution of Ge-Rh, the difference spectrum is also shown in Figure 6a. A small peak appeared

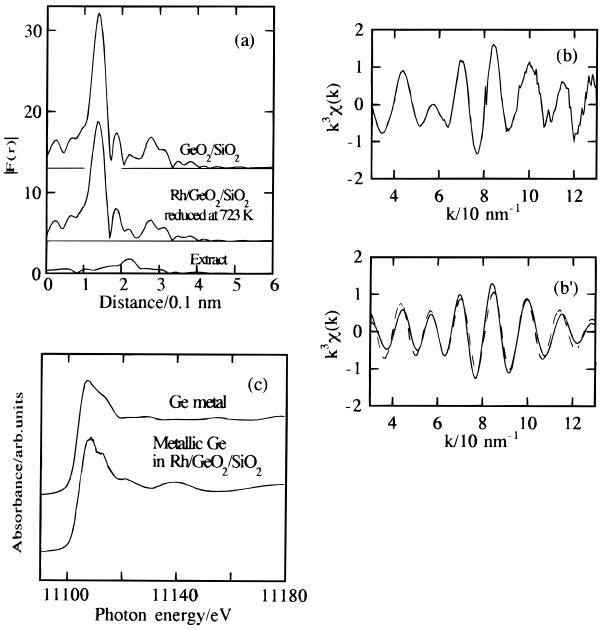

Figure 6. Ge K-edge XAFS spectra: (a) EXAFS Fourier transforms of one-atomic-layer GeO_2/SiO_2 and Rh/one-atomic-layer GeO_2/SiO_2 reduced at 723 K and their difference spectrum; (b) $k^3\chi(k)$ spectrum and (b′) curve fitting analysis with Ge−Rh single wave of the difference spectra of Rh/one-atomic-layer GeO_2/SiO_2 reduced at 723 K after subtraction of the Ge-O oscillation; (c) XANES spectra of Ge metal powder and the Rh/one-atomic-layer GeO_2/SiO_2 reduced at 723 K after subtraction of the one-atomic-layer GeO_2/SiO_2 spectrum.

in the difference EXAFS spectrum. The curve fitting analysis of the extracted spectrum by a Ge−Rh single wave gave a reasonable result, as shown in Figure 6b′. The fitted Ge−Rh distance is 0.243 nm (Table 2), which agrees well with the measurement at the Rh K-edge within experimental error. This result supports the RhGe alloy formation in the Rh/one-atomic-layer GeO_2/SiO_2 reduced at high temperature. The influence of RhGe alloy formation is also observed in the XANES spectrum of Figure 6c, where a small shoulder appeared. To see more clearly the shoulder structure, we subtracted the spectrum of one-atomic-layer GeO_2/SiO_2 from that of the Rh/one-atomic-layer GeO_2/SiO_2 reduced at 723 K. The position of the obtained difference spectrum in Figure 6c corresponds to that of metal Ge. Ge K-edge EXAFS for the Rh/one-atomic-layer GeO_2/SiO_2 reduced at 423 K was the same as that for one-atomic-layer GeO_2/SiO_2, suggesting no significant structural change of the one-atomic-layer GeO_2 at this reduction temperature.

As a consequence, $Rh_6(CO)_{16}$ is supported on the GeO_2/SiO_2 with retention of the cluster framework below 343 K, the supported $Rh_6(CO)_{16}$ clusters are converted to Rh metallic particles by reduction with H_2 at 423−523 K, and RhGe alloy particles are produced on one-atomic-layer GeO_2/SiO_2 by reduction above 623 K.

3.2. Catalytic Hydrogenation of Ethyl Acetate to Ethanol on Rh/One-Atomic-Layer GeO_2/SiO_2. Figure 7 shows the activity and selectivity of the catalytic hydrogenation of ethyl acetate on Rh/one-atomic-layer GeO_2/SiO_2 as a function of the prereduction temperature. For comparison, the results on Rh/c-GeO_2/SiO_2, Rh/GeO_2, and Rh/SiO_2 are also shown in Figure 7. Ideally, the reaction proceeds by eq 3.

$$CH_3COOC_2H_5 + 2H_2 \rightarrow 2C_2H_5OH \qquad (3)$$

The by-products in parallel reactions are acetaldehyde or hydrogenolysis products such as methane and ethane. The selectivity to ethanol (S_{C2H5OH}) is defined as carbon-base

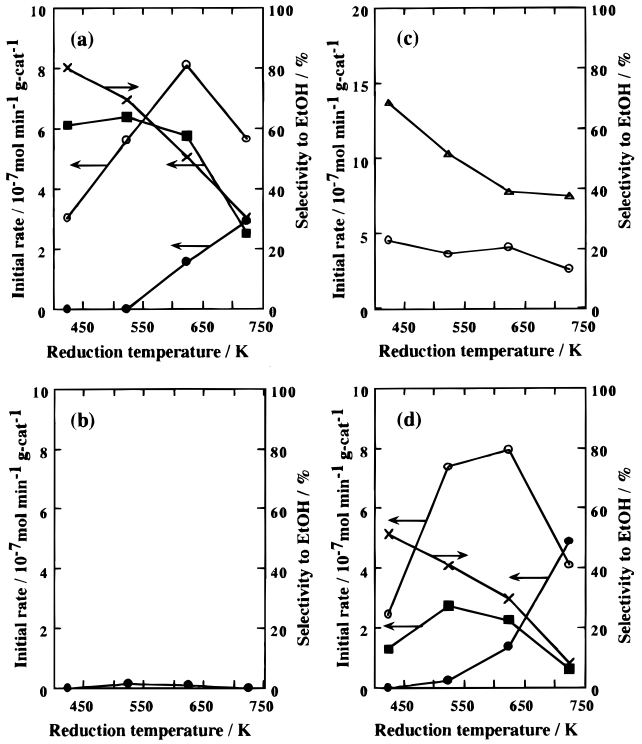

Figure 7. Catalytic activity and selectivity (ethanol formation) of (a) Rh/one-atomic-layer GeO_2/SiO_2, (b) Rh/bulk-GeO_2, (c) Rh/SiO_2, and (d) Rh/c-GeO_2/SiO_2 in catalytic hydrogenation of ethyl acetate plotted as a function of reduction temperature; reaction temperature 473 K, hydrogen pressure 6.6 kPa, ethyl acetate pressure 1.3 kPa: (■) ethanol, (●) acetaldehyde, (○) methane, (△) ethane, and (×) selectivity to ethanol.

selectivity, which is given by eq 4.

$$S_{C2H5OH} = \frac{r_{C2H5OH}}{r_{C2H5OH} + r_{CH3CHO} + (1/2)r_{CH4} + r_{C2H6}} \qquad (4)$$

r_{C2H5OH}, r_{CH3CHO}, r_{CH4}, and r_{C2H6} are the initial rates for the formation of C_2H_5OH, CH_3CHO, CH_4, and C_2H_6 in mol min^{-1} g-$cat.^{-1}$. The defined selectivity (eq 4) is equivalent to the selectivity defined by $r_{C2H5OH}/2r_{CH3COOC2H5}$, where $r_{CH3COOC2H5}$ is the initial rate of the ethyl acetate consumption.

Rh/one-atomic-layer GeO_2/SiO_2 showed the highest selectivity for ethanol formation when the catalyst was reduced at 423 K. The catalysts reduced at 423−523 K were most active for ethanol formation. In these catalysts, Rh is present as metallic particles on the one-atomic-layer GeO_2/SiO_2, as characterized by EXAFS. The activity and selectivity for ethanol formation successively decreased with a rise of prereduction temperature, as shown in Figure 7. It is to be noted that the ethanol formation proceeded selectively at such a low hydrogen pressure as 13.3 kPa, which is a considerably moderate condition for this kind of catalytic reaction compared with the conditions used on copper chromite or other catalysts thus far studied. Acetaldehyde as a by-product was produced on the Rh/one-atomic-layer GeO_2/SiO_2 reduced at 623 K, and the formation was enhanced by increasing prereduction temperature. The temperature of the beginning of acetaldehyde formation agreed with the temperature of the beginning of the RhGe alloy formation.

The catalytic reactions were compared with those on Rh/bulk-GeO_2 and Rh/SiO_2 in Figure 7. On Rh/GeO_2 very small amounts of acetaldehyde were detected over the whole temperature range. Thus it is ascertained that Rh/GeO_2 is inactive for ethyl acetate hydrogenation. The reason for the inactivity of Rh/GeO_2 is attributed to the dissolution of Rh into metallic

Ge generated by the reduction of GeO_2 surface to form RhGe alloy particles which are suggested to be located in the GeO_2 bulk and below the surface of GeO_2 support.[7] No adsorption of CO and H_2 was observed on the reduced Rh/GeO_2 samples. The TPD spectrum in Figure 4c showed a CO desorption peak at temperatures as low as 400 K, suggesting that the carbonyl ligands of $Rh_6(CO)_{16}$ on bulk GeO_2 desorb before the RhGe alloy formation.

On Rh/SiO_2 ethane and methane were major products in the whole temperature range of prereduction, and neither ethanol nor acetaldehyde was produced, as shown in Figure 7c. The total activity decreased with a rise of reduction temperature.

To examine the property of Rh particles on the one-atomic-layer GeO_2 supported on SiO_2 surface, we also compared the catalysis of Rh/one-atomic-layer GeO_2/SiO_2 with that of Rh/c-GeO_2/SiO_2. The c-GeO_2/SiO_2 is prepared by exposing the one-atomic-layer GeO_2/SiO_2 to 1.3 kPa of H_2O for 1 h at room temperature.[20] In the present study the Rh/one-atomic-layer GeO_2/SiO_2 reduced at 523 K was exposed to water vapor under similar conditions. The effect of the exposure of H_2O vapor on the Rh metal was examined by EXAFS, but the spectral feature did not change in both Fourier transform and $k^3\chi(k)$ oscillation spectra after exposure of H_2O vapor. The Rh−Rh coordination number determined by the curve fitting analysis for the Rh/c-GeO_2/SiO_2 was almost the same as that for the original 523 K-reduced Rh/one-atomic-layer GeO_2/SiO_2, as shown in Table 1. This means that the Rh metal does not suffer any effect by exposure to H_2O vapor. The activity and selectivity of the Rh/c-GeO_2/SiO_2 for ethyl acetate hydrogenation were plotted as a function of prereduction temperature in Figure 7d. A small change in the activity for the formation of methane and acetaldehyde was observed by transformation of the GeO_2 monolayer to the three-dimensional crystalline GeO_2 particles. A more drastic effect of the morphological change of GeO_2 on the catalysis was observed with the formation of ethanol, which was suppressed drastically by the crystallinity of GeO_2, as shown in Figure 7a,d. Thus, the formation of methane and acetaldehyde is insensitive to the morphology of GeO_2 on SiO_2, while ethanol is produced preferentially in the presence of the one-atomic-layer GeO_2 rather than the GeO_2 particles.

From these results, it is concluded that the most active phase for the ethanol formation from ethyl acetate is the combination of the Rh metallic particles and the one-atomic-layer GeO_2. The Rh particles themselves do not catalyze the selective ethanol formation because the Rh/SiO_2 catalysts were inactive for ethyl acetate hydrogenation (Figure 7c). The RhGe alloy particles produce acetaldehyde rather than ethanol.

To explore the role of the one-atomic-layer GeO_2 on SiO_2 in ethanol formation, FT-IR spectra of adsorbed ethyl acetate on the one-atomic-layer GeO_2/SiO_2 and SiO_2 were measured. Figure 8a shows the FT-IR spectra of the one-atomic-layer GeO_2/SiO_2 after exposure of 1.3 kPa of ethyl acetate at 373, 423, and 473 K, followed by evacuation of the gas phase at the same temperatures. The peaks are observed at 2980, 2934, 2901, 1728, 1391 and 1376 cm^{-1}. The bands at 2980, 2934, and 2901 cm^{-1} and 1391, and 1376 cm^{-1} are assigned to the CH stretching and CH bending vibrations, respectively. The band at 1728 cm^{-1} is assignable to the C−O stretching mode of unidentate acetate because it agrees with the spectrum of unidentate germyl acetate ester.[25] Thus the observed spectra indicate the dissociative adsorption of ethyl acetate to form unidentate acetate on the one-atomic-layer GeO_2/SiO_2. The peak intensity of the adsorbed species became more intense with an increase of adsorption temperature. Similar spectra were

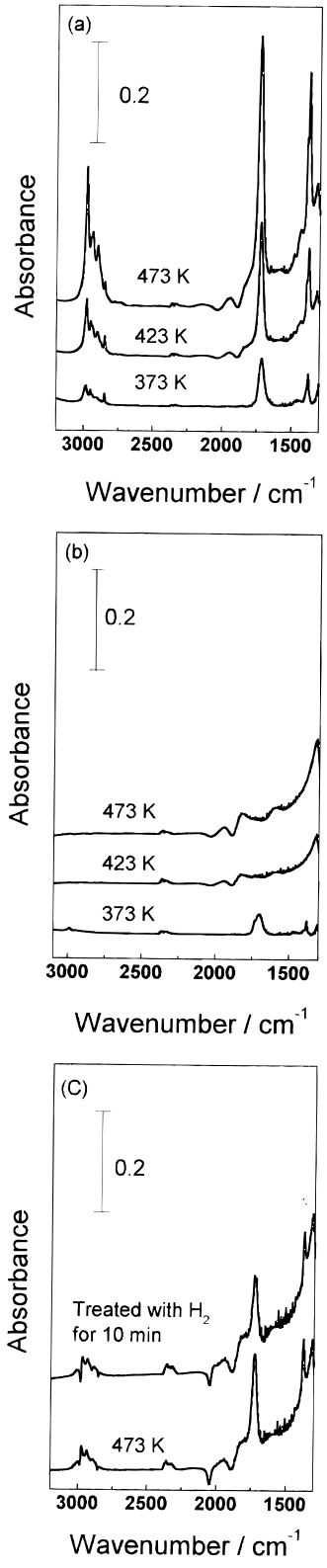

Figure 8. FT-IR spectra of ethyl acetate adsorbed on (a) one-atomic-layer GeO_2/SiO_2, (b) SiO_2, and (c) Rh/one-atomic-layer GeO_2/SiO_2. Spectra a and b were measured after exposure of 1.3 kPa of ethyl acetate at 373, 423, and 473 K, followed by evacuation of the gas phase at the same temperatures, respectively. Spectra c were the ones of ethyl acetate adsorbed on Rh/one-atomic-layer GeO_2/SiO_2 at 473 K and then treated with H2 for 10 min at 473 K.

observed under the catalytic reaction conditions on Rh/one-atomic-layer GeO_2/SiO_2 at 473 K, as shown in Figure 8c, and no other species was detected. The peak intensity of the adsorbed species on the GeO_2/SiO_2 without Rh remained

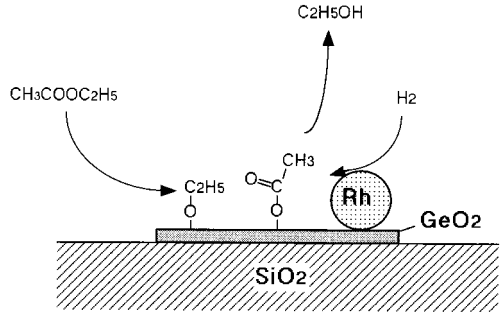

Figure 9. Schematic picture of ethyl acetate hydrogenation on Rh/one-atomic-layer GeO_2/SiO_2 reduced at 423−523 K.

unchanged under hydrogen at 473 K, whereas it readily reduced on Rh/one-atomic-layer GeO_2/SiO_2 by introducing H2 to the system (Figure 8c). Similar spectra were observed on bulk-GeO_2, which implies that the adsorption mode is inherent in GeO_2. Ethyl acetate dissociates to bidentate acetate and ethanol on TiO_2,[26,27] where the dissociation of ethyl acetate occurs on OH groups at the TiO_2 surface, which possesses Brönsted acidity. Considering the lack of surface acidity on GeO_2/SiO_2, it is plausible that the dissociative adsorption proceeds on Ge−O−Ge sites. Indeed, it has been demonstrated that the dissociative adsorption of acetic acid on GeO_2 was accompanied with scission of Ge−O−Ge bond to form germyl ester and isolated OH groups.[25] A similar explanation has been applied to the chemisorption of methanol on GeO_2.[28] Ethyl acetate may also adsorb on the Ge−O−Ge sites of the one-atomic-layer GeO_2 to form unidentate acetate and ethoxyl groups, as illustrated in Figure 9. On the other hand, ethyl acetate did not adsorb on SiO_2 as shown in Figure 8b.

From these results on the catalytic properties of Rh/one-atomic-layer GeO_2/SiO_2, Rh/crystalline GeO_2 particles/SiO_2, Rh/bulk-GeO_2, and Rh/SiO_2 and the characterization of the catalysts by EXAFS and FT-IR, a possible reaction mechanism of the ethyl acetate hydrogenation is stated as follows. Ethyl acetate dissociatively adsorbs to form unidentate acetate and ethoxy on the one-atomic-layer GeO_2, while hydrogen adsorbs on the Rh metallic particles supported on the GeO_2 overlayer to supply adsorbed hydrogen atoms. The hydrogen atoms are spilt over from the Rh particles to the one-atomic-layer GeO_2 on which the hydrogenation of the adsorbed species proceeds to produce ethanol, as illustrated in Figure 9. The Rh particles in Rh/one-atomic-layer GeO_2/SiO_2 may strongly interact with the one-atomic-layer GeO_2 because the ethane formation observed on Rh/SiO_2 was completely suppressed on Rh/one-atomic-layer GeO_2/SiO_2. At present, there is no evidence for the details of the metal−support interaction, electronic and/or decoration (GeO_x) effects. By reduction above 623 K RhGe alloy particles were formed, where the selectivity to ethanol decreased markedly.

4. Conclusions

(1) New Rh/one-atomic-layer GeO_2/SiO_2 catalysts were prepared by supporting $Rh_6(CO)_{16}$ on the one-atomic-layer GeO_2 attached on the SiO_2 surface, followed by reduction with H_2 at 423-723 K.

(2) The Rh/one-atomic-layer GeO_2/SiO_2 catalysts reduced at 423−523 K showed high activity and selectivity for ethyl acetate hydrogenation to produce ethanol. On the contrary, Rh/GeO_2 and Rh/SiO_2 were inactive for ethanol formation from ethyl acetate.

(3) The one-atomic-layer GeO_2 on SiO_2 was much more effective as a support for Rh metallic particles than three-dimensional GeO_2 particles dispersed on SiO_2.

(4) Structural change of $Rh_6(CO)_{16}$ on the one-atomic-layer GeO_2/SiO_2 was followed by EXAFS, TPD, and FT-IR. In the samples reduced below 343 K the $Rh_6(CO)_{16}$ cluster framework was retained. By reduction at 423−523 K the carbonyl ligands partially desorbed and metallic Rh particles were formed. By further reduction above 623 K RhGe alloy particles were formed.

(5) We proposed a schematic picture of the ethyl acetate hydrogenation on the Rh/one-atomic-layer GeO_2/SiO_2 catalyst reduced at 423−523 K in Figure 9. Ethyl acetate dissociatively adsorbs to form unidentate acetate and ethoxy on the one-atomic-layer GeO_2, which react with hydrogen atoms supplied through the Rh surface.

(6) This study demonstrates the significance of the use of the monolayer sample as a support for metal in the catalytic hydrogenation of ethyl acetate and exemplifies the advantageous applications of an inorganic oxide monolayer.

Acknowledgment. This work has been supported by CREST (Core Research fro Evolutional Science and Technology) of Japan Science and Technology Corporation (JST).

References and Notes

(1) Xie, Y.-C.; Tang, Y.-Q. *Adv. Catal.* **1990**, *37*, 1.

(2) Niwa, M. *Shokubai* **1992**, *34*, 221.

(3) Asakura, K.; Aoki, M.; Iwasawa, Y. *Catal. Lett.* **1988**, *1*, 395.

(4) Asakura, K.; Iwasawa, Y. *Chem. Lett.* **1986**, 859.

(5) Shirai, M.; Asakura, K.; Iwasawa, Y. *J. Phys. Chem.* **1991**, *95*, 9999.

(6) Asakura, K.; Iwasawa, Y. *Chem. Lett.* **1988**, 633.

(7) Okumura, K.; Asakura, K.; Iwasawa, Y. *J. Chem. Soc., Faraday Trans.*, in press.

(8) Galvagno, S.; Poltarzewski, Z.; Donato, A.; Neri, G.; Pietropaolo, R. *J. Chem. Soc., Chem. Commun.* **1986**, 1729.

(9) Marsden, W. L.; Wainwright, M. S.; Friedrich, J. B. *Ind. Eng. Chem. Prod. Res. Dev.* **1980**, *19*, 551.

(10) Shimizu, M.; Takeoka, S. *Bull. Chem. Soc. Jpn.* **1981**, *6*, 912.

(11) Evans, J. W.; Wainwright, M. S.; Cant, N. W.; Trimn, D. L. *J. Catal.* **1984**, *88*, 203.

(12) Evans, J. W.; Casey, P. S.; Wainwright, M. S.; Trimn, D. L.; Cant, N. W. *Appl. Catal.* **1983**, *7*, 31.

(13) Evans, J. W.; Cant, N. W.; Trimn, D. L.; Wainwright, M. S. *Appl. Catal.* **1983**, *6*, 355.

(14) Grey, R. A.; Pez, G. P.; Wallo, A.; Corsi, J. *J. Chem. Soc., Chem. Commun.* **1980**, 783.

(15) Mansour, A. E.; Candy, J. P.; Bournonvivlle, J. P.; Ferretti, O. A.; Basset, J.-M. *Angew. Chem., Int. Ed. Engl.* **1989**, *28*, 347.

(16) Candy, J. P.; Ferretti, O. A.; Mabilon, G.; Bournonville, J. P.; Mansour, A. E.; Basset, J.-M.; Martino, G. *J. Catal.* **1988**, *112*, 210.

(17) Whener, P. S.; Testin, G. C.; Gustafson, B. L. *J. Catal.* **1984**, *88*, 246.

(18) Deshpande, V. M.; Ramnarayan, K.; Narasimhan, C. S. *J. Catal.* **1990**, *121*, 174.

(19) Iijima, S.; Ichikawa, M. *J. Catal.* **1985**, *94*, 313.

(20) Okumura, K.; Asakura, K.; Iwasawa, Y., submitted.

(21) Asakura, K. In *X-ray Absorption Fine Structure for Catalysts and Surfaces*; Iwasawa, Y., Ed.; World Scientific: Singapore, 1996.

(22) McMaster, W. H.; Del Grande, Kerr N.; Mallet, N.; Hubell, J. H. *Comparison of X-ray Cross Section*; National Technical Information Service: Springfield, 1969.

(23) Bart, J. C. J. *Adv. Catal.* **1986**, *34*, 203.

(24) Grevans, G. N.; Durham, P. J.; Diakun, F.; Quinn, P. *Nature (London)* **1981**, *294*, 139.

(25) McManus, J. C.; Low, M. J. D. *J. Phys. Chem.* **1968**, *72*, 2378.

(26) Buckland, A. D.; Graham, J.; Rudham, R.; Rochester, C. H. *J. Chem. Soc., Faraday Trans.* **1981**, *77*, 2845.

(27) Graham, J.; Rochester, C. H.; Rudham, R. *J. Chem. Soc., Faraday Trans.* **1981**, *77*, 1973.

(28) McManus, J. C.; Matsushita, K.; Low, M. J. D. *Can. J. Chem.* **1969**, *47*, 1077.